Resonance State in ^{7}H

M. Caamaño,[1,2,*] D. Cortina-Gil,[1] W. Mittig,[2] H. Savajols,[2] M. Chartier,[3] C. E. Demonchy,[2] B. Fernández,[3] M. B. Gómez Hornillos,[3] A. Gillibert,[4] B. Jurado,[2] O. Kiselev,[5,6] R. Lemmon,[7] A. Obertelli,[4] F. Rejmund,[2] M. Rejmund,[2] P. Roussel-Chomaz,[2] and R. Wolski[8]

[1]*Department of Particle Physics, Universidade de Santiago de Compostela, E-15782, Santiago de Compostela, Spain*
[2]*GANIL CEA/DSM-CNRS/IN2P3, BP 55027, 14076 Caen Cedex 05, France*
[3]*Department of Physics, University of Liverpool, Oliver Loge Laboratory, L69 7ZE, United Kingdom*
[4]*CEA/DSM/DAPNIA, CEA Saclay, 91191 Gif sur Yvette Cedex, France*
[5]*Institute of Nuclear Chemistry, University of Mainz, 55128 Mainz, Germany*
[6]*PNPI, Gatchina 188300, Russia*
[7]*CCLRC Daresbury Laboratory, Warrington, Cheshire, WA4 4AD, United Kingdom*
[8]*Henryk Niewodniczański Institute of Nuclear Physics, ul. Radzikowskiego 152 31-342 Krakow, Poland*

(Received 8 February 2007; published 9 August 2007)

The existence of the ^{7}H nuclear system was investigated via a one-proton transfer reaction with a ^{8}He beam at 15.4A MeV and a ^{12}C gas target. The experimental setup was based on the active-target MAYA which allowed a complete reconstruction of the reaction kinematics. The existence of the ^{7}H was confirmed with the identification of seven events where the system was formed with a resonance energy of $0.57^{+0.42}_{-0.21}$ MeV above the $^{3}\mathrm{H} + 4n$ threshold and a resonance width of $0.09^{+0.94}_{-0.06}$ MeV. This study represents an unambiguous proof of the existence of the most neutron-proton unbalanced system presently found.

DOI: 10.1103/PhysRevLett.99.062502 PACS numbers: 27.20.+n, 25.60.Je, 25.70.Ef

A major goal in nuclear physics is to understand how nuclear stability and structure arise from the underlying interaction between individual nucleons. Systematic measurements of exotic nuclei are a valuable tool to test the present models, which are mainly based on properties of stable nuclear matter, and check the validity of their predictions extended to these nuclei not found in nature. Recent developments in the production of radioactive beams, as ISOL and in-flight techniques, bring new opportunities to study these nuclei. The study of resonances beyond the drip lines, the limits in number of neutrons and protons able to form a bound system, is relatively accessible for neutron-rich light nuclei, such as hydrogen and helium, where the limit is reached with the addition of only a few neutrons to the stable isotopes.

The case of light nuclei is also particularly interesting because the low number of involved nucleons allows the development of pioneering theoretical descriptions. Calculations in *ab initio* approaches [1,2], based on realistic nucleon-nucleon interaction, showed that three-body interactions are important and necessary to obtain a good agreement with experimental data. In other approaches, the loosely bound character of these nuclei was the base for a core coupled to individual nucleons [3], or cluster structures [4,5]. Coupling to continuum becomes also important [6] and hyperspherical functions methods showed to be successful in this region [7,8].

The experimental search for hydrogen isotopes heavier than tritium started more than 40 years ago [9]. However, the map of the superheavy hydrogen isotopes is presently far from being complete. Whereas experiments have reported the existence of ^{4}H, ^{5}H, and ^{6}H as resonances [10–14], their fundamental properties are not unambiguously determined. In this situation, the search for a new member of the isotopic chain aims to complete our knowledge on these problematics, such as the evolution of the binding energy with the number of neutrons. Moreover, the observation of a resonance in ^{7}H reveals the nuclear system with the most extreme neutron to proton ratio presently reached, with $N/Z = 6$, and the last member of the hydrogen isotopic chain.

Recent results from some of these approaches have predicted the existence of the ^{7}H resonance with a resonance energy above the $^{3}\mathrm{H} + 4n$ mass varying from around 1 MeV in a hyperspherical functions method approach [7] up to 7 MeV in an antisymmetrized molecular dynamics calculation [1]. In parallel, experimental studies performed by Korsheninnikov *et al.* [15] show a sharp increase in the $p(^{8}\mathrm{He}, pp)$ channel close to the $^{3}\mathrm{H} + 4n$ disintegration threshold, interpreted as a first tentative evidence of the existence of ^{7}H as a low lying resonance. Our work is a major step in this direction and represents a clear experimental proof of the existence of ^{7}H as a nuclear system along its characterization as a resonance.

The experiment was performed at GANIL (France) using the SPIRAL facility based on the Isotope Separation On Line (ISOL) technique [16] of beam production. A secondary beam of ^{8}He at 15.4A MeV with an intensity of $\sim 10^{4}$ pps was produced using a primary ^{13}C beam on a thick ^{12}C target. The ^{7}H system was then studied via the $^{12}\mathrm{C}(^{8}\mathrm{He}, ^{7}\mathrm{H} \rightarrow {}^{3}\mathrm{H} + 4n)^{13}\mathrm{N}$ transfer reaction.

The experimental setup used in the present experiment detected the charged particles involved in the reaction using the active-target MAYA [17], which is especially

well suited for detecting reaction products in a very low energy kinematic domain. This detector is a time-charge projection chamber where the detection gas also plays the role of reaction target. The beam particles and the reaction products ionize the gas along their paths. The electrons released in the ionization process drift toward the amplification area where they are accelerated around a plane of amplification wires after traversing a Frisch grid. The accelerated electrons ionize again the surrounding gas inducing a mirror charge in the pads of a segmented cathode placed below the wires. Measurements of the drift time and the charge induced on the segmented cathode enable a complete three-dimensional tracking of those reaction products that lose enough energy to be detected. A segmented wall of 20 cesium-iodide (CsI) crystals placed at forward angles detects those particles that do not stop inside the gas volume. The detection of a charged particle in any CsI detector was used for triggering the acquisition during the experiment. Two drift chambers located before MAYA are used as beam monitors. The nonreacting projectiles are stopped in a small metal cup at the end of MAYA. Figure 1 shows a schematic view of the experimental setup.

In a typical event where ^{7}H is produced, a ^{8}He projectile enters in the detector and transfers one proton to the nucleus of a ^{12}C atom of the gas, C_4H_{10} at 30 mbar, which corresponds to a target thickness of 3.2×10^{19} $^{12}C/cm^2$. The scattered ^{7}H decays immediately into ^{3}H with relatively high kinetic energy and four neutrons. The first step in the selection of the $^{12}C(^{8}He, ^{7}H \rightarrow ^{3}H + 4n)^{13}N$ channel consists in the coincident identification of the charged reaction products, tritium and nitrogen. The triton is stopped in the segmented CsI wall and identified via the relation between the total energy and the fast component of the CsI signal output, which is sensitive to the mass and charge of the particle [18] (Fig. 2). The nitrogen recoil, with a total energy between 3 and 15 MeV, corresponding to a range between 40 and 160 mm, is stopped inside the detector. The range and angle are measured using the charge image projected on the segmented cathode, with typical uncertainties of ± 2 mm and $\pm 5°$, respectively. The identification of the recoil is done by means of the relation

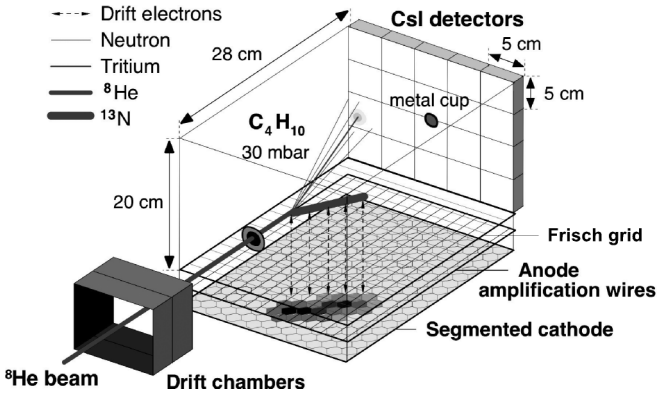

FIG. 1. Experimental setup. See text for details.

between the measured range and the deposited charge, which is a function of the total energy when the recoil is completely stopped inside the gas. The nitrogen total energy is then calculated from the measured range using the available code SRIM [19]. Figure 2 shows the selection of nitrogen among other recoil species by means of their different range over charge ratios. The largest peak corresponds to carbon isotopes mainly coming from elastic reactions. Higher range over charge ratios are populated with isotopes with lower charges, such as boron isotopes produced in $^{12}C(^{8}He, ^{x}Li)^{20-x}B$ reactions. The left peak corresponds to charges greater than carbon. In the present case the largest recoil charge detected in coincidence with any particle in the CsI wall corresponds to nitrogen isotopes. The inner gray histogram shows in Fig. 2 the distribution conditioned by the identification of a triton in the CsI wall. Counts corresponding to carbon isotopes still remain after the condition, mainly due to three-body reaction channels. However, the good separation in the carbon and nitrogen identification when the tritium coincidence is applied allows one to avoid contamination from these channels. The different $1p$-xn transfer reaction channels producing ^{3}H and a nitrogen recoil are separated afterwards by their different kinematics. Contributions from

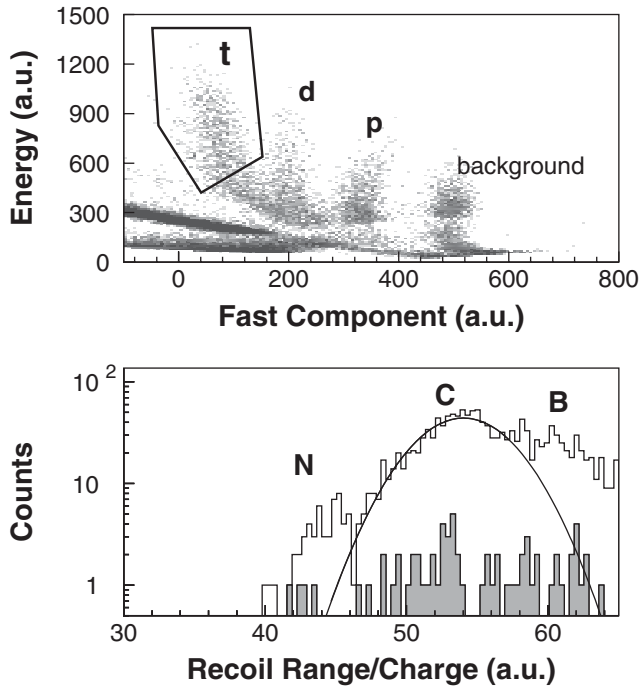

FIG. 2. Triton and nitrogen identification. Top panel: The selection of tritium among other hydrogen isotopes in the CsI detectors is shown with a solid line in energy versus fast component coordinates. Isotopes of helium populate the lines with energies below 300 and a fast component below 200. Bottom panel: The selection of nitrogen among other recoil species is shown in a spectrum of range/charge ratio. The carbon isotopes region is fitted to a Gaussian shape for reference. The gray histogram shows the distribution when conditioned by tritium identification in the CsI detectors.

other reaction channels, such as fusion evaporation, are eliminated with the coincident detection of a single recoil, identified as nitrogen, and a single scattered particle in the CsI wall, identified as a triton with relatively high energy.

The $^{12}C(^{8}He, ^{7}H)^{13}N$ one-proton transfer is a binary reaction with two particles in the final state. Conservation of energy and momentum allows one to reconstruct the reaction kinematics from the information of only one of the reaction products. In the present work, the reconstruction is done with the nitrogen recoil angles and energies measured with the three-dimensional tracking of MAYA. The kinematic information can be reduced to the excitation energy of the ^{7}H system applying a missing mass calculation. The excitation energy is then defined as the difference between the calculated mass of the ^{7}H system with respect to the reference $^{3}H + 4n$ subsystem mass.

The identification of the ^{7}H events is done after the identification of the events corresponding to other reaction channels with ^{3}H and nitrogen as products, such as ^{6}H and ^{5}H. The upper panel in Fig. 3 shows the excitation energy distribution corresponding to ^{5}H production. This is calculated assuming that the detected nitrogen is ^{15}N and the subsystem mass is $^{3}H + 2n$. Those events marked as a gray histogram lie on a region defined by the width of the ^{5}H resonance and centered in its energy, according to previous experiments [12,13], and they are associated to the ^{5}H channel. The middle panel shows the excitation energy distribution corresponding to ^{6}H production. The calculation was done assuming the detected nitrogen as ^{14}N and a $^{3}H + 3n$ subsystem mass. The events in the peak marked as a gray histogram are different from those associated with ^{5}H and lie on the region also defined by the ^{6}H resonance width and energy observed in previous experiments [14]. These events correspond to the ^{6}H channel. Finally, the lower panel shows the excitation energy distribution assuming the detected nitrogen as ^{13}N and the subsystem mass as $^{3}H + 4n$. The events lying on the peak marked in gray around the $^{3}H + 4n$ disintegration threshold are different from those previously associated to ^{5}H and ^{6}H channels. In addition, other reactions produced in the present experimental setup, such as fusion evaporation, are estimated to populate the kinematic region of the ^{7}H with less than one count after the ^{3}H + nitrogen selection. Estimations on the six-body $^{13}N + ^{3}H + 4n$ phase space of the ^{7}H channel, and phase space associated with ^{6}H and ^{5}H channels, result in a background contribution which begins to be appreciable around -10 MeV below the $^{3}H + 4n$ threshold. Under these considerations those events located in the marked region are identified as ^{7}H production reactions, resulting in seven events among the total data. The peaked distribution is a signature of a well-defined state and represents a background free confirmation of the production of the ^{7}H resonance.

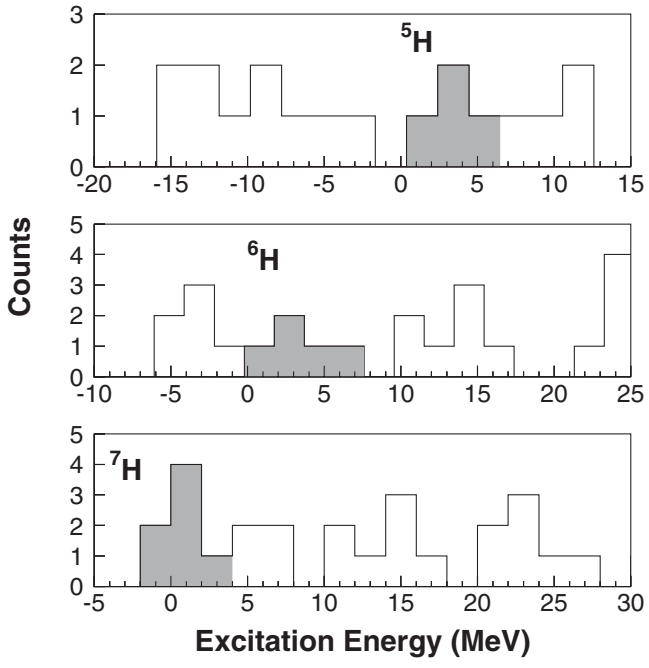

FIG. 3. Excitation energy distributions calculated under the assumptions of ^{5}H (top panel), ^{6}H (middle panel), and ^{7}H (bottom panel) production channels. The gray histograms in the ^{5}H and ^{6}H channels correspond to those events lying in the regions where the resonances were already observed in previous experiments. The gray histogram in the ^{7}H corresponds to those events identified as ^{7}H production. See text for details.

The low lying character of the resonance allows one to detect some events very close to the $^{3}H + 4n$ decay threshold, which then may appear at negative energies due to the uncertainty in the excitation energy reconstruction. The cross section of the ^{7}H production was determined as the number of detected ^{7}H events normalized to the number of incident projectiles and target nuclei. This calculation is corrected by the efficiency of the detection system. A mean differential cross section of $d\sigma/d\Omega = 40.1^{+58.0}_{-30.6}$ μb/sr was obtained within the angular coverage of MAYA, calculated as $9.7°-48.2°$ in the center-of-mass frame.

The peak in excitation energy corresponding to the production of ^{7}H (Fig. 4) is described in this work with a modified Breit-Wigner distribution [20],

$$\sigma_{\mathrm{BW}} = \sigma_0 \frac{\Gamma\sqrt{E^{\mathrm{exc}}/E_R}}{(E^{\mathrm{exc}} - E_R)^2 - (\Gamma^2/4)(E^{\mathrm{exc}}/E_R)} \qquad (1)$$

where the production cross section σ_{BW} depends on the excitation energy E^{exc} through the resonance energy E_R and width Γ. The formula includes a modification factor $\sqrt{E^{\mathrm{exc}}/E_R}$ to take into account energy dependence of the system barrier. The factor σ_0 is determined with the normalization to the total cross section.

The Breit-Wigner function is fitted to the experimental values of the excitation energy using a multiparametric maximum likelihood procedure [21], which is especially suited to low statistics samples.

The total likelihood is calculated in an event-by-event basis, multiplying the individual contributions. Each event contributes to the total likelihood as a Gaussian function

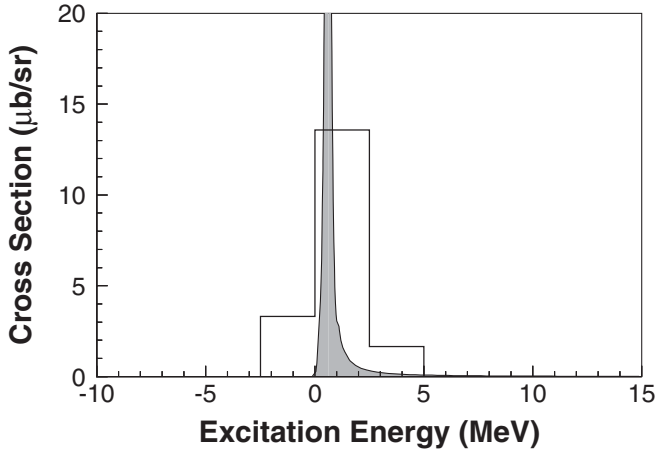

FIG. 4. Excitation energy distribution for the identified ^{7}H events. The solid function is the Breit-Wigner distribution resulting from the fit to the experimental events. The data are represented with the empty histogram merely as a guide to the eye, with a 2.5 MeV binning corresponding to the average estimated uncertainty.

centered in the measured excitation energy and with a variance equal to its calculated uncertainty, convoluted and normalized with the Breit-Wigner distribution. The energy and width of the resonance are scanned until the maximum likelihood is found. The uncertainty associated to each event is mainly dominated by the tracking reconstruction process, resulting in an average value of 2.5 MeV. The contribution of the estimated uncertainty is mainly reflected in the error bars associated to the resonance width calculated by the likelihood procedure.

The fitted parameters result in a width of $\Gamma = 0.09^{+0.94}_{-0.06}$ MeV, and a resonance energy of $E_R = 0.57^{+0.42}_{-0.21}$ MeV above the threshold of the $^3\mathrm{H} + 4n$ subsystem. In Fig. 4 the fitted Breit-Wigner distribution is displayed with the experimental excitation energy distribution of the ^{7}H detected events.

The previous experimental observation of Korsheninnikov *et al.* [15], where a sharp increase of the cross section appeared close to the $^3\mathrm{H} + 4n$ threshold, is in qualitative agreement with the resonance energy evaluated in this work. Regarding theoretical descriptions, calculations based on a hyperspherical functions method applied on a shell model basis are closest to the present work [7,8], even though the predicted resonance energies range between 1 MeV [7] and 3 MeV [8]. In any case, it is difficult to conclude that this is the most appropriate description due to the lack of predictions for ^{7}H from other approaches.

Some estimations of the resonance width resulted in theoretical values 3 orders of magnitude lower than the present work [22], while phase-shift correlations suggest a width around some mega-electron volt for the present resonance energy. Being the resonance width related to the decay rate and mechanism, the relatively low value extracted in this work may be a hint of a fast and unique four-neutron decay [15,23]. Future studies of the ^{7}H nuclear state structure may bring more information about a possible 4-neutron cluster, also interesting for the current discussion about the existence of tetraneutron (^4n) state [24,25].

The present results constitute a major step forward in the study of the most exotic nuclear systems ever found, showing that nuclear matter with N/Z up to 6 can still exist. They also provide essential input for developing theoretical descriptions, improving our general understanding of nuclear matter.

This work was supported by grants from the Spanish Ministry of Education and Science, project No. FPA2005-00732, the CICYT-IN2P3 cooperation, and the Marie Curie Actions program support. The authors wish to thank deeply Dr. A. Navin for valuable discussions during the writing of this Letter.

*caamano@ganil.fr

[1] S. Aoyama and N. Itagaki, Nucl. Phys. **A738**, 362 (2004).
[2] P. Navrátil, J. Vary, and B. Barrett, Phys. Rev. Lett. **84**, 5728 (2000).
[3] G. Blanchon, A. Bonaccorso, and N. Vinh Mau, Nucl. Phys. **A739**, 259 (2004).
[4] P. Descouvemont and A. Kharbach, Phys. Rev. C **63**, 027001 (2001).
[5] K. Arai, Phys. Rev. C **68**, 034303 (2003).
[6] A. Volya and V. Zelevinsky, Phys. Rev. Lett. **94**, 052501 (2005).
[7] N. K. Timofeyuk, Phys. Rev. C **65**, 064306 (2002).
[8] N. K. Timofeyuk, Phys. Rev. C **69**, 034336 (2004).
[9] E. Argan *et al.*, Phys. Rev. Lett. **9**, 405 (1962).
[10] A. V. Belozyorov *et al.*, Nucl. Phys. **A460**, 352 (1986).
[11] S. I. Sidorchuk *et al.*, Phys. Lett. B **594**, 54 (2004).
[12] M. Meister *et al.*, Phys. Rev. Lett. **91**, 162504 (2003).
[13] A. A. Korsheninnikov *et al.*, Phys. Rev. Lett. **87**, 092501 (2001).
[14] D. Aleksandrov *et al.*, Sov. J. Nucl. Phys. **39**, 323 (1984).
[15] A. A. Korsheninnikov *et al.*, Phys. Rev. Lett. **90**, 082501 (2003).
[16] A. C. C. Villari *et al.*, Nucl. Phys. **A588**, c267 (1995).
[17] W. Mittig *et al.*, Nucl. Phys. **A722**, C10 (2003).
[18] G. F. Knoll, *Radiation Detection and Measurement* (John Wiley and Sons, New York, 1989).
[19] J. F. Ziegler, 2005, http://www.srim.org.
[20] G. Breit and E. Wigner, Phys. Rev. **49**, 519 (1936).
[21] M. Caamaño, Ph.D. thesis, Universidade de Santiago de Compostela, 2006.
[22] M. S. Golovkov *et al.*, Phys. Lett. B **588**, 163 (2004).
[23] A. A. Korsheninnikov, Nucl. Phys. **A751**, 501c (2005).
[24] F. M. Marqués *et al.*, Phys. Rev. C **65**, 044006 (2002).
[25] S. C. Pieper, Phys. Rev. Lett. **90**, 252501 (2003).